

Check for updates

www.afm-journal.de

Drug-Eluting Shear-Thinning Hydrogel for the Delivery of Chemo- and Immunotherapeutic Agents for the Treatment of Hepatocellular Carcinoma

Natashya Falcone, Menekse Ermis, Ankit Gangrade, Auveen Choroomi, Patric Young, Tess G. Mathes, Mahsa Monirizad, Fatemeh Zehtabi, Marvin Mecwan, Marco Rodriguez, Yangzhi Zhu, Youngjoo Byun, Ali Khademhosseini,* Natan Roberto de Barros,* and Han-Jun Kim*

Hepatocellular carcinoma (HCC) is a malignant and deadly form of liver cancer with limited treatment options. Transcatheter arterial chemoembolization, a procedure that delivers embolic and chemotherapeutic agents through blood vessels, is a promising cancer treatment strategy. However, it still faces limitations, such as inefficient agent delivery and the inability to address tumor-induced immunosuppression. Here, a drug-eluting shear-thinning hydrogel (DESTH) loaded with chemotherapeutic and immunotherapeutic agents in nanocomposite hydrogels composed of gelatin and nanoclays is presented as a therapeutic strategy for a catheter-based endovascular anticancer approach. DESTH is manually deliverable using a conventional needle and catheter. In addition, drug release studies show a sustained and pH-dependent co-delivery of the chemotherapy doxorubicin (acidic pH) and the immune-checkpoint inhibitor aPD-1 (neutral pH). In a mouse liver tumor model, the DESTH-based chemo/immunotherapy combination has the highest survival rate and smallest residual tumor size. Finally, immunofluorescence analysis confirms that DESTH application enhances cell death and increases intratumoral infiltration of cytotoxic T-cells. In conclusion, the results show that DESTH, which enables efficient ischemic tumor cell death and effective co-delivery of chemo- and immunotherapeutic agents, may have the potential to be an effective therapeutic modality in the treatment of HCC.

N. Falcone, M. Ermis, A. Gangrade, A. Choroomi, P. Young, T. G. Mathes, M. Monirizad, F. Zehtabi, M. Mecwan, M. Rodriguez, Y. Zhu, A. Khademhosseini, N. R. de Barros, H.-J. Kim
Terasaki Institute for Biomedical Innovation (TIBI)
Los Angeles, CA 90024, USA
E-mail: khademh@terasaki.org; nbarros@terasaki.org; hanjun@korea.ac.kr
Y. Byun, H.-J. Kim
Department of Pathophysiology and Preclinical Science
College of Pharmacy
Korea University
30019 Sejong, Republic of Korea
H.-J. Kim
Vellore Institute of Technology (VIT)

The ORCID identification number(s) for the author(s) of this article

can be found under https://doi.org/10.1002/adfm.202309069

DOI: 10.1002/adfm.202309069

1. Introduction

Hepatocellular carcinoma (HCC) is a type of liver cancer and a leading cause of cancerrelated mortality worldwide.[1,2] It is estimated that more than one million new HCC cases will be diagnosed by 2025,[2] contributing to more than one million deaths in 2030.[1] HCC treatment remains challenging due to late diagnosis and a lack of therapeutic options for advanced disease.[3,4] For example, surgical resection and liver transplantation are the most radical approaches; however, they are only indicated in cases of early diagnosis, usually due to tumor size. Even then, up to 70% of patients experience recurrence within 5 years.^[5] This highlights the limitations of current surgical interventions and underscores the necessity for alternative therapeutic options for advancedstage HCC. While historically, systemic chemotherapy has been the cornerstone of cancer treatment, the inability to achieve uniform drug delivery to tumors, collateral toxicity to the healthy liver tissues, and systemic side effects have provided

a reason for interest in developing novel the rapies or platforms for liver cancer. $\sp[3]$

Transcatheter arterial chemoembolization (TACE) is a promising procedure for treating liver cancer. This technique involves using an X-ray-guided catheter to deliver microbeads loaded with chemotherapy directly into the artery vessels supplying liver tumors. [6–10] However, the embolization efficiency is relatively low as the beads cannot be readily delivered into microvasculature to achieve uniform ischemia and chemotherapy delivery. [7,11] This non-uniformity can impede the desired therapeutic effect and reduce the overall efficacy of the procedure. Another limitation is that these beads can break apart or aggregate in blood vessels, preventing them from traveling deeper into tumors. [12] In addition, TACE today does not address cancer-mediated immune suppression.

www.afm-journal.de

1616238, 2024, 8, Downloaded from https://dvanced.orn/inelibrary.wiley.com/doi/0.1002/afm.202309069 by Korea University Library. Wiley Online Library on [2309/2025]. See the Terms and Conditions (https://onlinelibrary.wiley.com/erms-and-conditions) on Wiley Online Library for rules of use; OA articles are governed by the applicable Creative Commons Licross

Recently, novel immunotherapeutic agents, including immune checkpoint inhibitors (ICIs), CAR-T cells, and oncolytic viruses, have been developed and used to treat various cancers.[13-16] However, their use is still limited due to systemic side effects and difficulty delivering to solid tumors.^[17] ICI therapy, in particular, has revolutionized cancer treatments in recent years and dramatically improved cancer outcomes. [18,19] They target specific proteins expressed in cancer or immune cells, allowing the immune system to recognize and attack cancer cells more effectively. Specifically, some block the PD-1/PD-L1 interaction between T cells and cancer cells to overcome T cell exhaustion. [20] Others bind to CTLA-4 to allow for robust activation of T cells.^[21]

Unlike traditional chemotherapy or targeted therapies, ICIs can elicit durable patient responses.^[22] The activated immune cells can continue recognizing and attacking cancer cells even after the treatment is completed, leading to long-term responses. However, some systemic side effects can arise from the activation of the immune system, leading to immune-related adverse events that may affect healthy tissues.^[23] Strategies to minimize systemic side effects and improve tumor-specific delivery of these agents are necessary to harness the full potential of immunotherapy in liver cancer treatment and can be achieved with drug delivery systems. Furthermore, poor tumor penetration and the tumor immunosuppressive microenvironment lead to a low response rate of about 30% in patients treated with ICIs. [24] Therefore, relieving the immunosuppressive microenvironment has been explored with combination therapies.^[25,26]

Synergistic effects of chemotherapy and immunotherapy can lead to improved outcomes and increased patient response rates.[27] Chemotherapy exerts its effects by inducing cell death through apoptosis and inhibiting the cell cycle, reducing tumor growth. [28] Additionally, chemotherapy triggers an intense inflammatory response in the tumor microenvironment (TME).[29] It has been reported that some chemotherapeutics, such as doxorubicin (DOX), can induce dendritic cell maturation and infiltration of T cells into the tumor, thus turning the "cold" immunosuppressive tumor into a "hot" tumor. [30] This, in turn, promotes immunogenic cell death (ICD) and enhances the recognition and response of the immune system against cancer cells.[31] DOX induces reactive oxygen species (ROS)-based endoplasmic reticulum stress effects for ICD induction.[32] Therefore, it is used in this study to alter the TME to be more susceptible to immunotherapy. However, a drug delivery system that allows for a sustained release and can deliver the therapies locally to the tumor is ideal for minimizing the systemic side effects and delivering the therapeutics locally to the tumor.[10,25,33-35] Hydrogel biomaterials are a leading class of delivery matrices that can be used. Hydrogel biomaterials offer several advantages as delivery systems in cancer therapy. The tunable physical and chemical properties of hydrogels allow for customization to suit specific therapeutic requirements.^[36,37] Additionally, hydrogels allow for a targeted and sustained delivery of therapeutics while minimizing off-target effects.[38]

Shear-thinning hydrogels (STHs) are biomaterials with injectability properties resulting from decreased viscosity under shear stress and recovery once the stress is removed.[38-40] They can be crosslinked through physical crosslinking, such as ionic, hydrophobic, hydrogen bonding, and electrostatic interactions. [41] These interactions can be broken and reformed

based on external stimuli, allowing for these shear-thinning properties. Based on these unique mechanical characteristics, the STHs can be administered through needles or catheters to deliver the therapeutic agents locally and sustainably, leading to long-term effects and thus eliminating the need for multiple injection doses.[42] Among the various STHs, nanocomposite hydrogels based on electrostatic interactions have been consistently reported to have high applicability due to their simplicity of preparation and injectability based on their shear thinning properties.^[43] Hydrogels produced with the synthetic nanoclay Laponite have gained attention due to their unique shearthinning properties, making them suitable for easy injection and delivery through needles and catheters for various biomedical applications.[41] When mixed with gelatin, Laponite forms hydrogels with strong electrostatic interactions and can be used for controlled drug release. [38,42,44] In prior studies from our group, this hydrogel has been used to achieve a pH-dependent drug (DOX) release controlled through electrostatic attraction/repulsion, hydrogen bonding, and ionic exchange between the drug and Laponite.[42]

In this study, we present a transformative technology that uses a catheter-based locoregional approach to deliver a shearthinning gelatin/nanoclay composite hydrogel, that is, nextgeneration TACE, to induce more efficient ischemic cell death within the tumor microvasculature coupled with efficient chemoand immunotherapy delivery. The drug-eluting shear-thinning hydrogel (DESTH) can be delivered manually with conventional needles and catheters to induce ischemic cell death efficiently. Additionally, an effective co-delivery of chemo- and immunotherapy agents demonstrates the potential of our DESTH as a valuable and transformative option in advancing HCC therapies.

2. Results and Discussion

2.1. Preparation and Characterization of the Shear-Thinning **Biomaterials**

In this study, we aimed to develop a tunable biocompatible DESTH, which can be delivered by a catheter to liver lesions with deep penetration and solidify upon reaching the target vessel size, releasing entrapped chemo- and immunotherapeutic agents in a sustained and localized manner for treating HCC (Figure 1). Building upon previous reports demonstrating the potential of localized chemotherapy in converting tumors from an immunosuppressive "cold" state to an immunogenic "hot" state, we sought to enhance immunotherapeutic responses in HCC.^[45]

STHs were prepared by combining Laponite with gelatin solution. Three STH formulations were prepared using altering concentrations of gelatin and Laponite, 6NC25, 6NC50, and 6NC75 (6 corresponding to the concentration in weight percentage of overall gel and NC25-75 representing the percentage of Laponite within the mixture). The shear-thinning and mechanical properties were characterized using rheology and injection force measurements. Shear-thinning properties define flow behavior under shear forces and recovery of the hydrogel after the force is removed. Shear thinning is required for delivering hydrogels using syringes and catheters, so the STHs must be easy to administer while maintaining their properties during the injection. Therefore, injection force measurements were performed using

16163028, 2024. 8, Downloaded from https://advanced.onlinelibrary.wiley.com/doi/10.1002/adfm.202309069 by Korea University Library, Wiley Online Library on [23/09/2025]. See the Terms and Conditions (https://onlinelibrary.wiley.com/erms

and-conditions) on Wiley Online Library for rules of use; OA articles are governed by the applicable Creative Commons

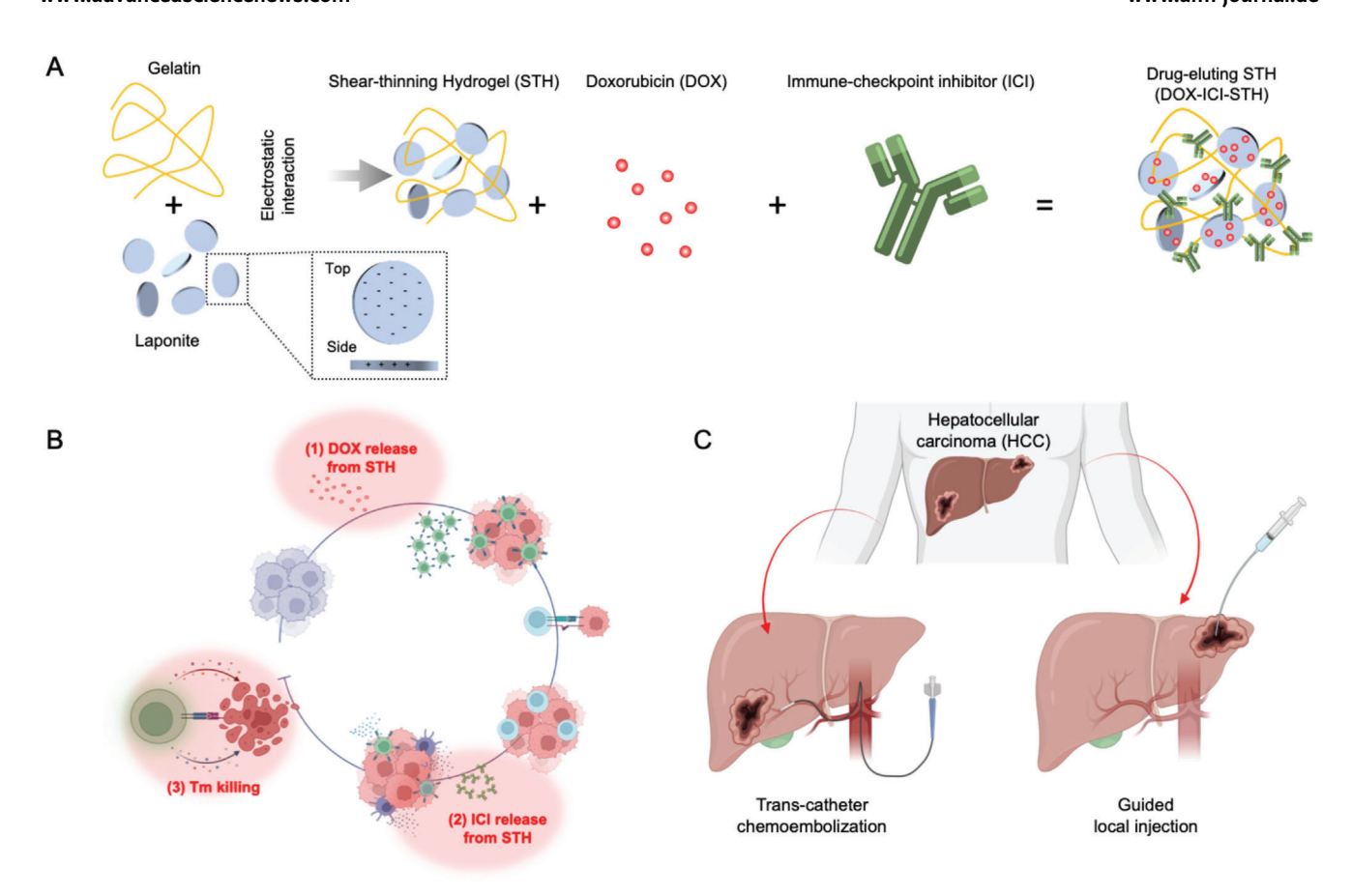


Figure 1. Schematic combination therapy: chemotherapy and immunotherapy within a DESTH. A) Preparation of gelatin/Laponite STH and loading DOX and ICI (aPD1) into the hydrogels. B) The mode of action of combined chemo- and immunotherapy on HCC. C) STHs can be delivered through a catheter using the TACE method or direct injection into the tumor vicinity.

a 1CC syringe with a 2.8 Fr catheter and a 3CC syringe with a 5 Fr catheter for the STHs described above (Figure 2A,B). It was found that STH 6NC25 (composite having the lowest Laponite concentration and highest gelatin) was the easiest to inject, having a load of \approx 8 N (1 cc/2.8 Fr) and 15 N (3 cc/5 Fr), compared to 6NC50 and 6NC75 (composite having the highest Laponite concentration and the lowest gelatin), with a load of 20-25 N (1 cc/2.8 Fr) and 28-34 N (3 cc/5 Fr) (Figure 2C,D). At higher concentrations of Laponite, the colloid network becomes more robust and less prone to shear-thinning because of increased interactions between the nanosilicate particles (i.e., electrostatic and van der Waal forces). This aligns with literature that states that hydrogels have lower concentrations of Lapointe to gelatin, resulting in the nanocomposites retaining the viscoelastic properties of gelatin, creating a more viscous, sheer-thinning hydrogel. [44,46] These results showed that as the Laponite concentration in the STH was increased, the force required to inject the hydrogel also increased.

From the rheological studies of the STHs, the storage modulus was measured, as well as the recovery after exposure to strain and viscosity (Figure 2E). Under conditions where the shear rate is greater than or equal to 0.1/s, 6NC25 displayed the lowest viscosity, meaning a lower resistance to mechanical deformation and flow (Figure 2Eii). However, our results showed that at low shear rates (0.001 to 0.01 (1/s)), the shear stress and viscosity of some 6NC50s were higher than those of 6NC25. The shearthinning properties were shown for all concentrations of hydrogels (Figure 2Ei,iii). These results proved that Laponite is the major component contributing to mechanical properties. Additional results from injectability and rheology are presented in the Supporting Information (Figures S1 and S2, Supporting Information).

In our previous rheology (shear stress, viscosity) results of drug-free STH, 6NC25 showed lower shear stress and viscosity than 6NC50 at lower shear rates.^[44] However, the injection force plateau of 6NC25 is significantly lower than the 6NC50 for all injection conditions (1cc syringe+2.8Fr catheter, 3cc syringe+5Fr catheter). In particular, the force/pressure applied to hydrogelbased embolic agents in typical TACE applications is significant, suggesting that the drug-loaded 6NC25 may require less force for injection than the 6NC50 in real-world TACE application conditions.

2.2. Release of Chemo- and Immunotherapeutic Agents from **STHs**

The gelatin-Laponite hydrogel has previously been shown to release DOX in a pH-dependent matter as the DOX release increased as the pH decreased.[42] It was found that STHs with lower Laponite (6NC25) have a more significant release profile at www.advancedsciencenews.com

www.afm-journal.de

16163028, 2024, 8, Downloaded from https://advanced.onlinelibrary.wiley.com/doi/10.1002/adfm.202309069 by Korea University Library, Wiley Online Library on [23/09/2025]. See the Terms and Conditions (https://onlinelibrary.wiley.com/

conditions) on Wiley Online Library for rules of use; OA articles are governed by the applicable Creative Commons License

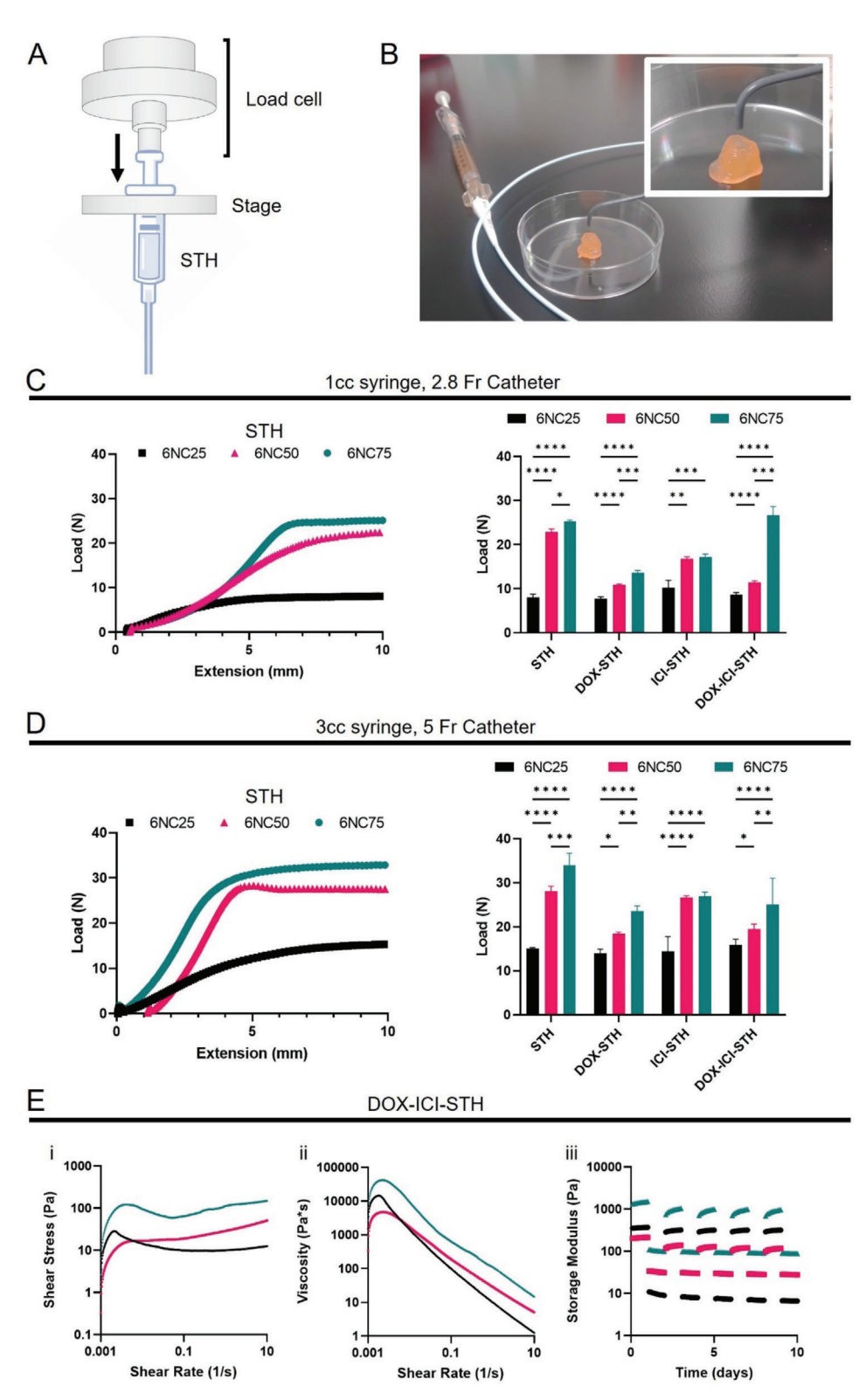


Figure 2. The mechanical properties of STHs encapsulated with DOX and aPD-1. A) The scheme for injectability testing of STHs using a syringe, catheter, and mechanical tester. B) Consistency of the STH after injection showing gelation post-shear-thinning. C) Injection force measurements of 6NC25, 6NC50, and 6NC75 formulations using a 2.8 Fr catheter and 1 cc syringe. D) Injection force measurements of 6NC25, 6NC50, and 6NC75 formulations using a 5 Fr catheter and 3 cc syringe. E) Rheological characterization of storage modulus, viscosity, and oscillatory step strains of 6NC25, 6NC50, and 6NC75 DESTH formulations.

16163028, 2024, 8, Downloaded from https://advanced.onlinelibrary.wiley.com/doi/10.1002/adfm.202309069 by Korea University Library, Wiley Online Library on [23/09/2025]. See the Terms and Conditions (https://onlinelibrary.wiley.com/doi/10.1002/adfm.202309069 by Korea University Library, Wiley Online Library on [23/09/2025]. See the Terms and Conditions (https://onlinelibrary.wiley.com/doi/10.1002/adfm.202309069 by Korea University Library, Wiley Online Library on [23/09/2025]. See the Terms and Conditions (https://onlinelibrary.wiley.com/doi/10.1002/adfm.202309069 by Korea University Library, Wiley Online Library on [23/09/2025]. See the Terms and Conditions (https://onlinelibrary.wiley.com/doi/10.1002/adfm.202309069 by Korea University Library, Wiley Online Library on [23/09/2025]. See the Terms and Conditions (https://onlinelibrary.wiley.com/doi/10.1002/adfm.202309069 by Korea University Library, Wiley Online Library on [23/09/2025]. See the Terms and Conditions (https://onlinelibrary.wiley.com/doi/10.1002/adfm.202309069 by Korea University Library.wiley.com/doi/10.1002/adfm.202309069 by Korea University Library.wiley.com/doi/10.1002/adfm.202309 by Morea University Library.wiley.com/doi/10.1002/adfm.202309 by Morea University Library.wiley.com/doi/10.1002/adfm.202309 by Morea University Library.wiley.com/doi/10.1002/adfm.202309 by Morea University Library.wiley.com/doi/10.1002/adfm.202309

conditions) on Wiley Online Library for rules of use; OA articles are governed by the applicable Creative Commons

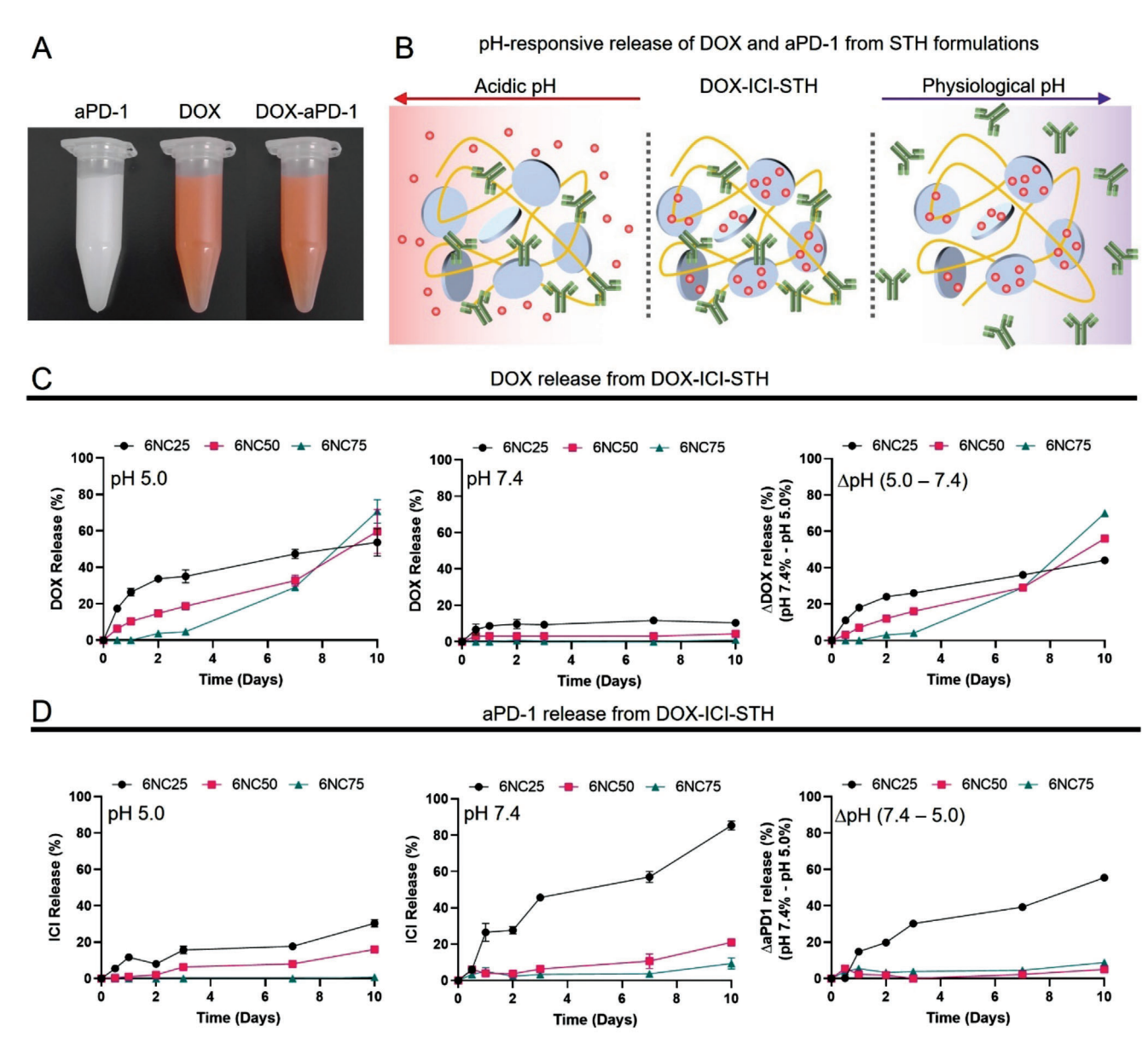


Figure 3. Drug release study of aPD-1 and DOX from STHs. A) Hydrogels prepared with aPD-1, DOX, and DOX-aPD-1. B) Scheme of the pH-responsive release of the combined immunotherapy. C) Release of DOX from 6NC25, 6NC50, and 6NC75 DOX-ICI-STH at pH 5.0 and 7.4. D) Release of aPD-1 from 6NC25, 6NC50, and 6NC75 DOX-ICI-STH at pH 5.0 and 7.4.

pH 5–6, followed by 6NC50 and 6NC75. Laponite is a synthetic nanoclay composed of layered silicates, and its strong electrostatic interactions with other charged species are made possible by the ensuing negative and positive charges on the surface of Laponite particles. These electrostatic interactions are responsible for the retention and release of drugs from the matrix and the pH-responsive behavior of Laponite (**Figure 3B**). At neutral pH (around pH 7), Laponite nanoparticles exhibit a strong negative charge due to the dissociation of hydroxyl groups on their surface, and as the pH is decreased, the concentration of hydrogen ions (H⁺) increases, leading to protonation of the surface hydroxyl groups resulting in a shift toward the positive charge. These strong interactions keep the hydrogel intact and contribute to the strong mechanical properties of the STH. Over the course

of testing, very minimal degradation of the hydrogel was observed.

STHs loaded with DOX and aPD-1 were tested at pH 5 and 7.4 (Figure 3C,D). Composite hydrogels containing lower concentrations of Laponite (6NC25) were shown to release about 35% of loaded DOX in 2 to 3 days at acidic pH. In contrast, STHs with higher Laponite concentrations released less than 20% for 6NC50 and less than 5% for 6NC75 (Figure 3C). However, after 3 days of exposure to the acidic environment, DOX release from STHs was increased, reaching up to 70% drug release in up to 10 days. Laponite has been known to degrade under acidic conditions, [48] which could also explain the increased release of DOX after 3 days of exposure to acidic pH. While Laponite may degrade to some extent in mildly acidic conditions, the extent of this degradation

1616208.2024, 8, Downloaded from https://alvanced.onlinelibrary.wiley.com/doi/10.1002/aff.202399069 by Korea University Library. Wiley Online Library on [23/09/2025]. See the Terms and Conditions (https://onlinelibrary.wiley.com/erms-and-conditions) on Wiley Online Library for rules of use; OA articles are governed by the applicable Certain Commons.

ADVANCED FUNCTIONAL MATERIALS

may not be significant enough to produce harmful by-products or significantly influence cells in the context of drug delivery, and the FDA has approved this formulation. At neutral pH, all STH compositions were shown to release less than 10% of loaded DOX by 2 to 3 days. In addition, no increased drug release was observed for extended incubation periods.

The average charge of DOX is positive at acidic pH, shifting to neutral as the pH increases to neutral, and is negatively charged at basic pH. Therefore, pH 5–6 represents a point where the DOX and Laponite have the same charge, increasing the release of the drug. Interestingly, aPD-1, a protein larger than DOX, has the opposite effects and releases more in physiological pH while still releasing in acidic pH (Figure 3D). All STH formulations tested were shown to provide a sustained release of aPD-1, with acidic environments providing a release of about 30% of aPD-1 up to 10 days for 6CN25, 18% for 6CN50, and less than 5% for 6CN75. In contrast, at neutral pH, aPD-1 release was improved and reached about 85% release up to 10 days for 6CN25, 20% for 6CN50, and 10% for 6CN75.

Protein drug release from Laponite involves the interplay of diffusion, desorption, and matrix degradation. [43] The pHresponsive effect of Laponite has been reported in a number of papers. There are reports that Laponite-based hydrogels can have yield stresses that change with pH changes.^[49] In addition, various researchers, including our previous paper, have reported that hydrogels containing Laponite are pHresponsive and can release drugs. [42,46,50,51] Due to the charges on Laponite, the interactions between the protein, which displays positively and negatively charged regions on its surface, can play a role in its binding and release. Furthermore, Laponite can expand, which creates channels or pores within the hydrogel, enabling the release of aPD-1 over time. However, to the best of our knowledge, it has not been fully investigated: 1) Laponite-based hydrogels loaded with more than one drug, or 2) proteins such as antibodies being released in response to pH changes.

The ideal immunotherapeutic TACE was considered to be one in which chemotherapeutic DOX is released first to convert the tumor to a "hot" tumor, followed by the release of immunotherapeutic agents to establish a second line of therapeutic defense. The STH allows for the slow, sustained release of the agents in a timely matter for the most optimal defense against cancer. It also shows a similar trend where 6NC25 shows the most release for aPD-1, followed by 6NC50 and 6NC75. The highest release kinetics observed in 6NC25 could be explained by the lower Laponite concentration, hence lower overall charge and matrix interactions in the hydrogel.

2.3. DOX-STH In Vitro Studies

Chemotherapy response can vary depending on the type and stage of cancer. Some cancers are more responsive to chemotherapy and have higher response rates. On the other hand, certain cancers are known to be less responsive to chemotherapy, meaning that the tumors may not shrink significantly or may continue to grow despite treatment. Examples of cancers that are typically less responsive to chemotherapy include pancreatic, liver, and some types of lung cancer.

was shown ineffective in the systemic treatment of HCC, and it is still the first drug of choice in TACE.^[54]

While it is shown that DOX released from STH has been effective in our past study in melanoma cancer, [42] here we observe different effects on liver cancer. Our DOX-STH in vitro studies show that release from an embolizing agent is not as effective for this type of cancer, and an extra line of treatment is needed. During this study, we exposed the DOX-STH media eluates with various concentrations of released DOX to the HepG2 cells over 7 days to evaluate the effects of the released DOX (Figure 4A,B). Consistent with the release studies, 6NC25 has the highest killing and decreased metabolic activity due to the highest release in comparison with the other gels. Additionally, only the highest concentration of DOX loaded in the STH 6CN25 (1000 µg mL⁻¹) has a significative effect (Figure 4B), achieving the IC₅₀ for DOX when used to treat HepG2 cells in vitro, which ranges from 1.6 to 14.4 µm depending on the treatment time.^[55] In contrast, all the other doses do not directly kill the liver cancer cells (i.e., do not achieve a DOX release enough to reach the IC_{50} for HepG2).

Furthermore, our results highlight the importance of considering the specific experimental setup when evaluating the effects of treatments. It is worth noting that the experimental conditions, specifically using samples tested in a neutral pH environment, may affect DOX release. The release of DOX was observed to be reduced at neutral pH (Figure 3C), which could also explain the diminished effect on liver cancer cells in vitro. Considering the experimental conditions, including pH, STH composition, and drug concentration, is essential for interpreting and optimizing the outcomes of such studies. Therefore, further investigations exploring combination therapy with ICIs are suggested to enhance the antitumor efficacy of DOX release.

While we show that DOX released from STHs is insufficient to kill the HepG2 cells directly, we investigated the ability of DOX to cause an increase in the expression of tumor markers. Immunohistochemistry analysis was performed on HepG2 cells after exposure to DOX-STH to evaluate the effect of DOX on the cells. The samples were stained for IFN-γ and PD-L1, and the fluorescence was measured from the confocal microscope images for up to 7 days (**Figure 5**). It was found that both PD-L1 and IFN- γ protein expression was increased over time in the STH and DOX-STH treated groups, with DOX-STH showing the highest fluorescence intensity of the surface markers after 7 days. When incubating HepG2 cells with DOX-STHs, we found an increase in the PD-L1 expression in the treated cancer cells, further supporting the benefit of dual treatment with chemo- and immunotherapies to make the tumor a good target for ICI treatment (Figure 5B). Comparing day 7 of our control group of media, STH alone, and the DOX-STH, we found the highest PD-L1 expression for DOX-STH. Additionally, IFN- γ detection increased after exposing the cells to DOX-STHs compared to media alone (control) and the STH after 7 days (Figure 5C). There is a trend in the STH and DOX-STH groups where the expression increases over time. In contrast, the control group stays relatively constant. In addition, the expression of IFN- γ in the DOX-STH group is the highest, showing the effect of DOX on the HepG2 cells.

It is known that DOX enhances the accumulation of IFN- γ in tumors. When cancer cells release more IFN- γ , it induces the expression of resistant genes in the cancer cells. While IFN- γ can induce immunoevasion and inhibition of antitumor

16163028, 2024, 8, Downloaded from https://advanced.onlinelibrary.wiley.com/doi/10.1002/adfm.202309069 by Korea University Library, Wiley Online Library on [23/09/2025]. See the Terms and Conditions (https://onlinelibrary.wiley

ions) on Wiley Online Library for rules of use; OA articles are governed by the applicable Creative Commons

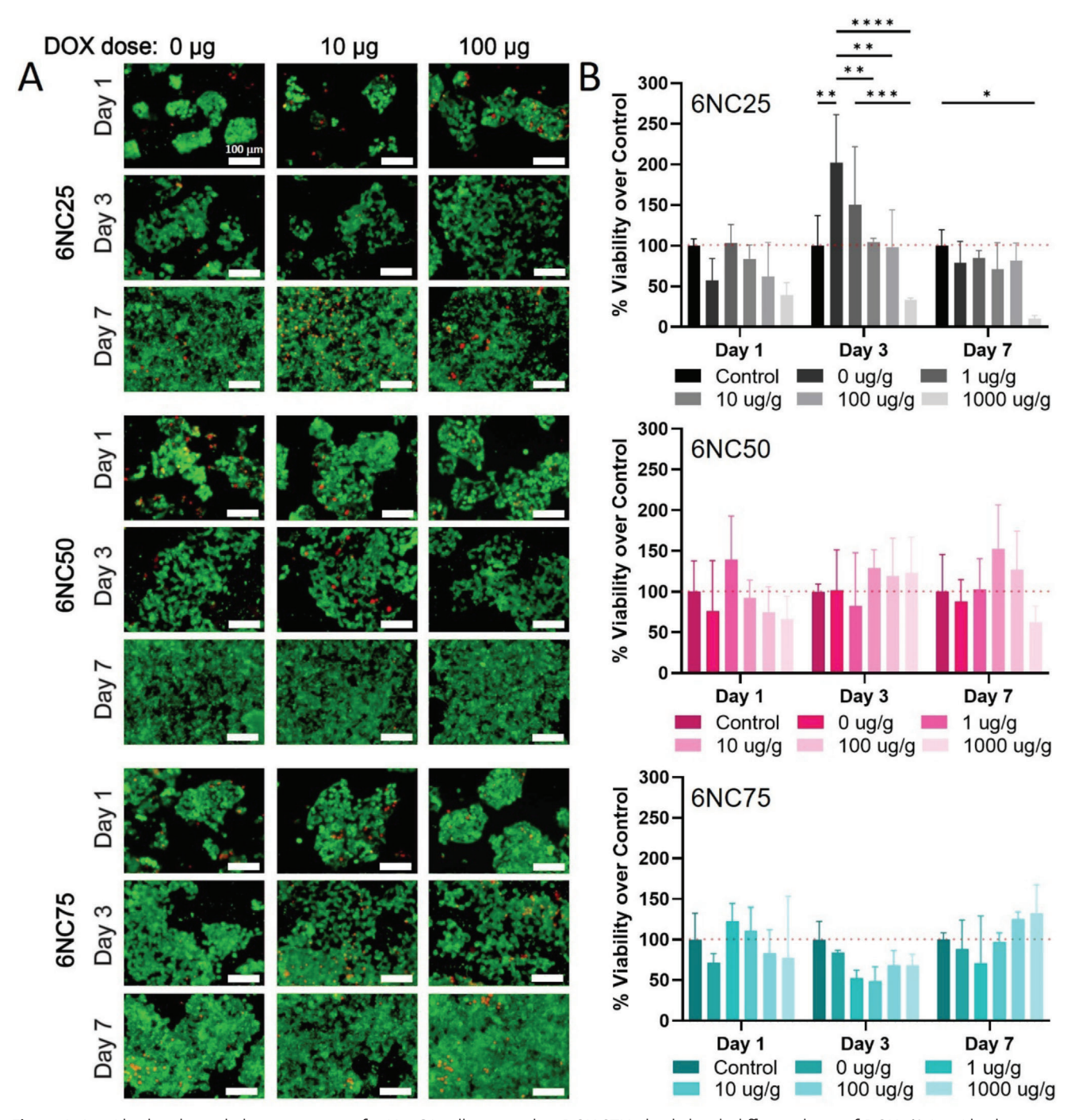


Figure 4. Live/dead and metabolic activity assay for HepG2 cells exposed to DOX-STHs loaded with different doses of DOX. A) Live/dead staining of HepG2 cells treated with 0, 1, 10, 100, and 1000 $\mu g \, g^{-1}$ DOX loaded 6NC25, 6NC50, and 6NC75 STHs (green: live; red: dead, scale bar: 100 μ m). B) PrestoBlue viability assay of the HepG2 cells cultured for 7 days and treated with STHs loaded with 0, 1, 10, 100, and 1000 $\mu g \, g^{-1}$ DOX, and no hydrogel control (grey: 6NC25, pink: 6NC50, blue: 6NC75). The dotted red line shows the viability % for the control group.

immunity, this signaling is also said to drive the maturation of immune cells and enhance T-cell infiltration, converting a "cold" tumor into a "hot" tumor, thus making immunotherapy more effective. Furthermore, DOX affects PD-L1 expression in cancer cells depending on the pathway activation and type of cancer. Upregulated PD-L1 expression in liver cancer may produce an im-

munosuppressive environment that impairs the capacity of the immune system to identify and destroy tumor cells. High PD-L1 expression can impair effector T cell performance and hasten their depletion, preventing them from efficiently identifying and killing cancer cells.^[57] The high expression of PD-L1 in liver cancer also offers a chance for immunotherapy, specifically immune

16163028, 2024. 8, Downloaded from https://advanced.onlinelibrary.wiley.com/doi/10.1002/adfm.202309069 by Korea University Library, Wiley Online Library on [23/09/2025]. See the Terms and Conditions (https://onlinelibrary.wiley.com/terms-

and-conditions) on Wiley Online Library for rules of use; OA articles are governed by the applicable Creative Commons

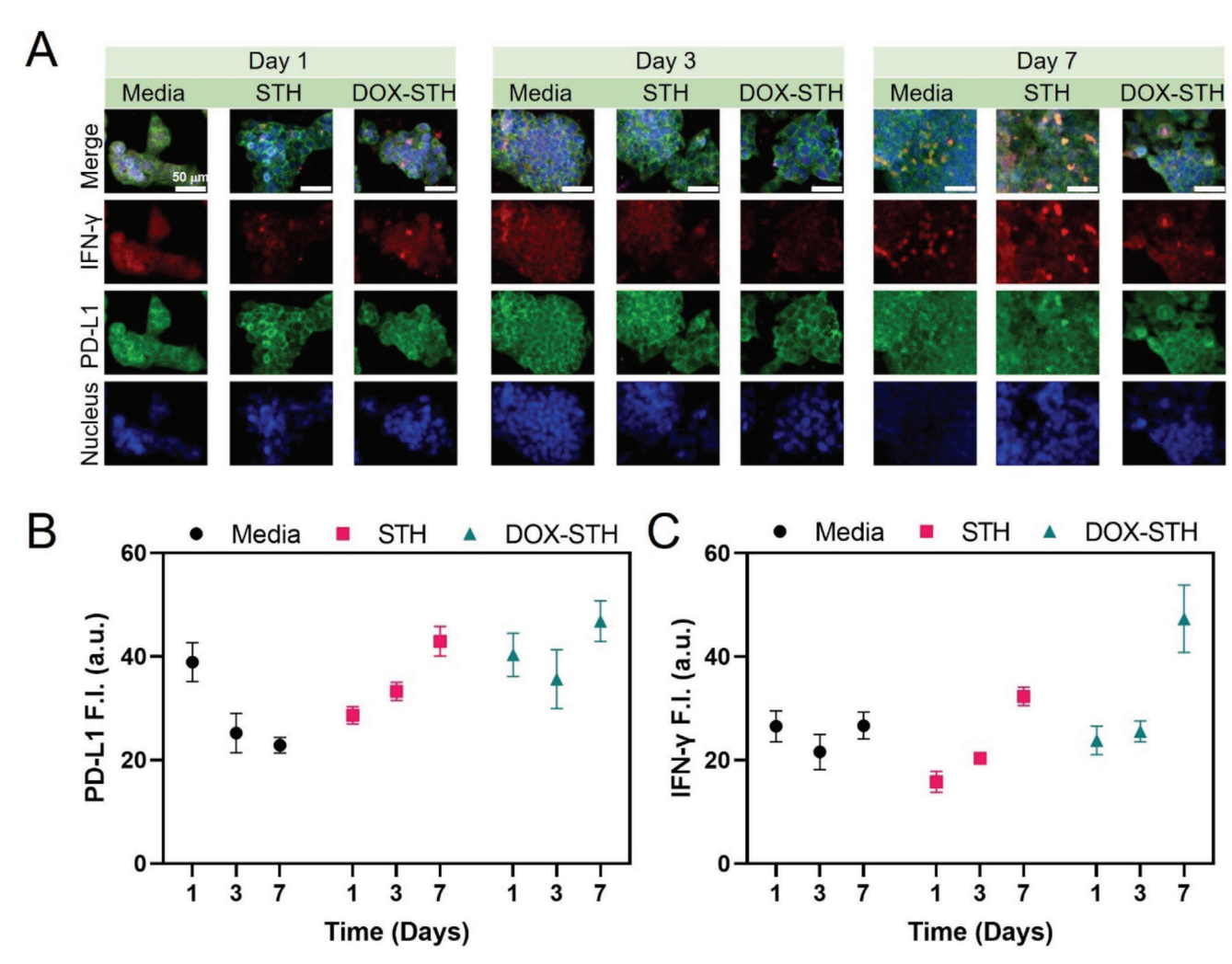


Figure 5. Immunostaining analysis of HepG2 cells exposed to DOX-STH at different time points. A) Immunostaining of HepG2 treated with 100 μg g^{-1} DOX. The samples were stained with aIFN- γ and aPD-L1 (blue: nucleus, red: IFN- γ , green: PD-L1, scale bar: 50 μm). B) PD-L1 fluorescence intensity measured from confocal laser scanning microscope (CLSM) images of HepG2 on days 1, 3, and 7 after media control, STH, and DOX-STH treatment. C) IFN- γ fluorescence intensity measured from CLSM images of HepG2 on days 1, 3, and 7 after media control, STH, and DOX-STH treatment.

checkpoint blocking therapy, making this type of cancer prone to ICIs, specifically aPD-1 or aPD-L1 antibodies. Immunotherapies that target the PD-1/PD-L1 pathway can interfere with the PD-1/PD-L1 interaction and restore the antitumor immune response. These treatments can increase the activity of effector T cells and improve their capacity to identify and destroy cancer cells by inhibiting the PD-1 receptor or PD-L1 ligand. Here, we show that DOX released from the STH may induce an increase in the immunotherapy treatment efficacy following DOX release.

2.4. In Vitro Release Study of aPD-1 from DOX-ICI-STHs with CHO PD1 Cell Line

Our next goal was to evaluate the release profile and binding potential of ICI protein released from ICI-STHs in vitro. While there are studies showing the release of ICIs from hydrogels and in vivo testing showing efficacy, proof that they can be delivered from STHs and bind to its PD-1 target on cancer cells has never been demonstrated in vitro. Therefore, a release study was conducted with a specialty CHO PD-1 overexpressing cell line (ATCC) to test the efficacy of releasing the aPD-1 protein from STHs. This reporter cell line has an abundance of PD-1 receptors in the cell surface for interaction with the aPD-1 released from the STHs. The binding of aPD-1 to its PD-1 receptor on CHO cells can be demonstrated by the successful delivery of aPD-1 from the hydrogel. The anti-mouse IgG then binds to the aPD-1, resulting in the emission of green fluorescence (Alexa488) (Figure 6A).

Results from the flow cytometer exhibit that the most significant binding events occurred with 6NC25, followed by 6NC50, and then 6NC75 of our composition of DOX-ICI-STH (Figure 6B,D). 6NC25 DOX-ICI-STH shows the most significant and fastest release rate, as saturation is apparent in the release from days 3 and 7, followed by 6NC50 DOX-ICI-STH. 6NC75 DOX-ICI-STH exhibited the lowest release due to the electrostatic

16163028, 2024, 8, Downloaded from https://advanced.onlinelibrary.wiley.com/doi/10.1002/adfm.202309069 by Korea University Library, Wiley Online Library on [23/09/2025]. See the Terms and Conditions

ns) on Wiley Online Library for rules of use; OA articles are governed by the applicable Creative Commons

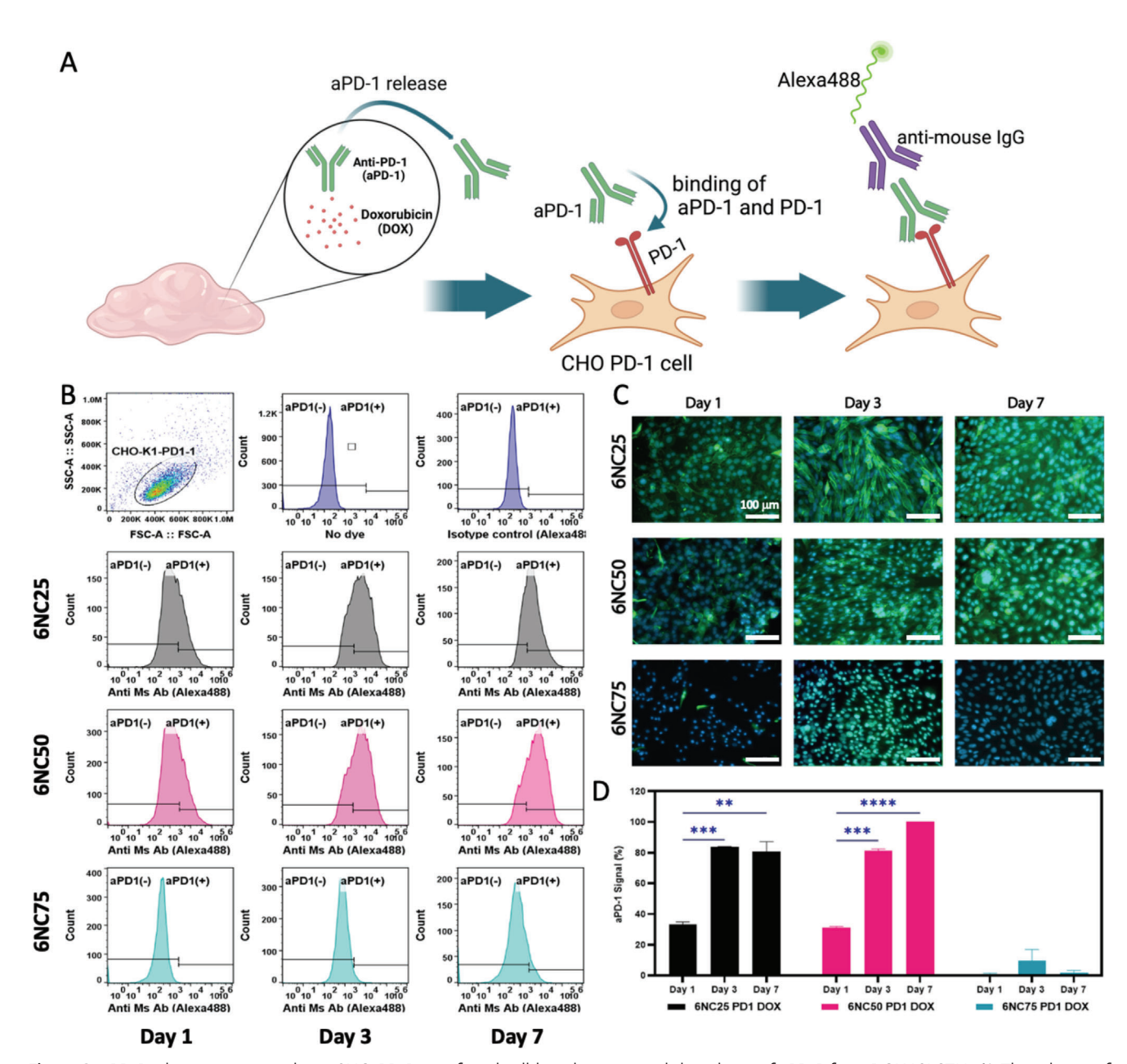


Figure 6. aPD-1 release in vitro study on CHO PD-1 transfected cell line demonstrated the release of aPD-1 from DOX-ICI-STH. A) The scheme of released aPD-1 detection using CHO PD-1 cells. B) Flow cytometer plots of CHO-PD-1 cells treated with aPD-1 loaded 6NC25, 6NC50, and 6NC75 STHs (n=3, representative images). C) Fluorescent microscopy images of CHO PD-1 cells treated with aPD-1 loaded 6NC25, 6NC50, and 6NC75 STHs (n=3, representative images) (nucleus: blue, green: aPD-1/anti-mouse IgG/Alexa488 complex, scale bar: 100 μ m). D) Quantification of aPD-1 binding to CHO PD-1 cell line.

interactions resulting from the higher Laponite concentration in the formulation.

Complementary imaging was done to confirm these results further (Figure 6C). The cells were stained using DAPI and antimouse IgG, with the binding of the aPD-1 to the cells shown through green fluorescence. For both 6NC25 DOX-ICI-STH and 6NC50 DOX-ICI-STH, the most significant amount of fluorescence was seen on day 7, as confirmed by the flow cytometry results (Figure 6D). Minimal fluorescence was seen for 6NC75 because of its previously mentioned slower release. These re-

sults demonstrate the successful and functional release of the aPD-1 antibodies from STHs and effective binding to the reporter cell line in a concentration-dependent manner. These results also agree with the drug release studies from STHs in which we observed the highest release from the 6NC25 composite (lowest Laponite concentration). The importance of this study lies in the fact that the aPD-1 antibodies released from the hydrogel still hold their functional integrity and interact with the PD-1 receptors on the cell surface in a physiological manner.

www.afm-journal.de

16163028, 2024, 8, Downloaded from https://advanced.onlinelibrary.wiley.com/doi/10.1002/adfm.202309069 by Korea University Library, Wiley Online Library on [23/09/2025]. See the Terms and Conditions (https://onlinelibrary.wiley.com/erms

and-conditions) on Wiley Online Library for rules of use; OA articles are governed by the applicable Creative Commons

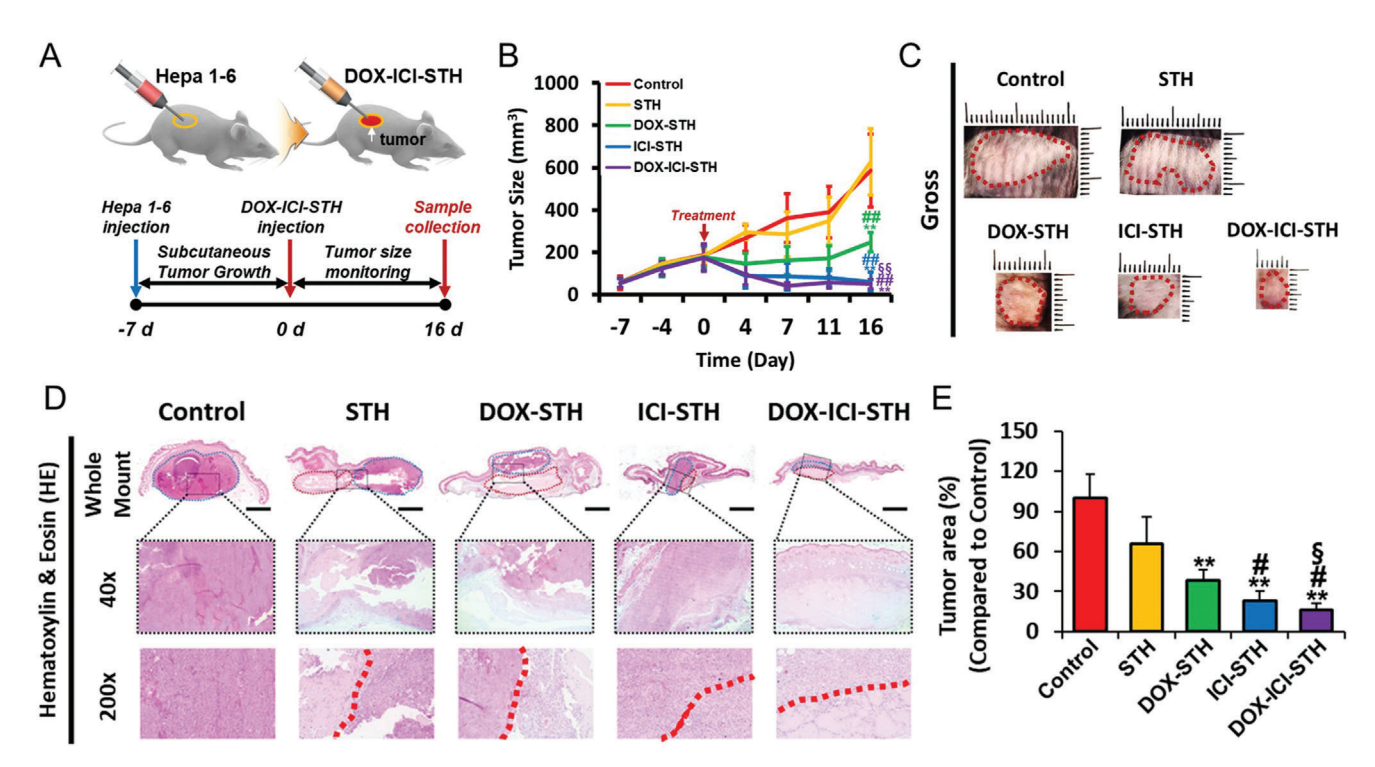


Figure 7. In vivo anticancer efficacy studies of DESTH on Hepa 1-6 tumor model. A) Experimental design of the in vivo tumor growth study. B) Tumor growth curve of DESTH treatments in Hepa 1-6 mouse tumor model. *p < 0.05, **p < 0.01, ANOVA (*: compared to control, #: compared to STH, and \$: compared to DOX-STH). C) Endpoint tumor gross images of experimental groups. The red dotted line: tumor D) Histopathological analysis of Hepa 1-6 mouse tumor models treated with DESTHs (DOX, ICI, DOX-ICI). Blue dotted line in the whole mount: tumor, red dotted line in the whole mount: STH remnant. The red dotted line in 200x: the border between the tumor and STH. Scale bar is 2 mm, 500, and 100 μ m for whole mount, 40x, and 200x, respectively. E) Quantitative analysis of tumor area. *p < 0.05, **p < 0.01, ANOVA (*: compared to control, #: compared to STH, and \$: compared to DOX-STH).

2.5. Anticancer Efficacy Testing Using a Mouse Liver Tumor Model

Our results from drug release studies confirmed that DOX and aPD-1 are released at different times depending on the composition of STH. We conducted experiments in a mouse liver tumor model to further analyze the in vivo anticancer efficacy of STH-based chemotherapeutic and immunotherapeutic delivery. The combined anticancer efficacy of DOX-ICI-STH is designed to induce immune cell infiltration and tumor cell killing in addition to the chemotherapeutic effectiveness of causing direct cell death. Therefore, we used a syngeneic model (mouse tumor cell implantation to mouse) rather than human liver cancer cells with nude mice to confirm the immunotherapeutic efficacy, which is responsible for one axis of the combined anticancer efficacy. For this purpose, mouse liver tumor cells (Hepa 1-6) were injected subcutaneously into 8-week-old male C57Bl/6J mice. Two sets of in vivo efficacy tests (survival and tumor growth study) were performed independently using the Hepa 1-6 tumor model (Figure 7A, Figure S6A, Supporting Information). In the Kaplan-Meier survival analysis, the tumor-only (control) and vehicle control (STH) groups died earlier than the treatment groups (DOX-STH, ICI-STH, DOX-ICI-STH) (Figure S6B, Supporting Information).

Interestingly, the DOX-STH group had a survival rate of less than 50% at the endpoint (day 16 post-treatment), while the DOX-

ICI-STH group had a much higher survival rate for most of the experimental period. However, the ICI-STH group had a lower survival rate than the DOX-ICI-STH group and still presented a 60% survival rate at the endpoint. The higher survival rate seen in the ICI-delivery group may be due to the fact that the Hepa 1-6 tumor model reported in the literature is known to have relatively high ICI sensitivity.^[58]

Tumor growth curve analysis was performed to confirm the anticancer efficacy of DOX-ICI-STH in the tumor growth process (Figure 7B,C). The tumor size of the control (PBS) and STH groups was larger than that of the treatment groups (DOX-STH, ICI-STH, DOX-ICI-STH) at the endpoint (post-treatment day 16) (Figure 7C). In the tumor growth curve, similar to the survival curve results, the DOX-ICI-STH group's tumor size was the smallest among the experimental groups (Figure 7B). There was no significant difference in tumor size between the DOX-ICI-STH and ICI-STH groups. However, the ICI-STH group did not show a statistically significant tumor size difference from the DOX-STH group. The DOX-ICI-STH group was significantly smaller than the DOX-STH group. In particular, the DOX-STH group showed an increase in tumor size at the endpoint. In contrast, the ICI-loaded groups (ICI-STH, DOX-ICI-STH) showed a constant size with no increase over time.

In addition to survival and tumor size studies, tumor samples were processed through the formalin-fixed paraffin-embedded method, followed by histopathological analysis with hematoxylin

ADVANCED FUNCTIONAL MATERIALS 16163028, 2024. 8, Downloaded from https://advanced.onlinelibrary.wiley.com/doi/10.1002/adfm.202309069 by Korea University Library, Wiley Online Library on [23/09/2025]. See the Terms and Conditions (https://onlinelibrary.wiley.com/terms-

and-conditions) on Wiley Online Library for rules of use; OA articles are governed by the applicable Creative Commons

& eosin (HE) staining to analyze the microstructural changes of Hepa 1-6 tumor model upon drug-loaded hydrogel treatment (Figure 7D.E). In the whole mount view of the macroscopic analysis results, all STH-treated groups (STH, DOX-STH, ICI-STH, DOX-ICI-STH) were observed to have residual injected STH material. Interestingly, in the DOX-ICI-STH group, the amount of STH remaining was more significant than the area occupied by the tumor. In the STH group, the boundary between the injected material and the tumor was relatively clear (Figure 7D, red dotted line). In contrast, DOX-STH was observed to have inflammatory cell infiltration between the material and the tumor. However, the infiltration of inflammatory cells inside the DOX-STH was less evident compared with ICI-loaded groups (ICI-STH and DOX-ICI-STH). In the ICI-STH and DOX-ICI-STH groups, the boundary between the tumor and drug-loaded STHs was unclear at high magnification (200x), and a large number of inflammatory cells were observed infiltrating the injected material. These results may indicate that the ICI-loaded material may affect immune cell migration and tumor infiltration. In addition, the tumor-only area, excluding the STH remnant, was analyzed (Figure 7E). Quantitative analysis showed that the size of tumors in the control and STH groups were not significantly different and were larger than the other drug-loaded groups (DOX-STH, ICI-STH, DOX-ICI-STH). In particular, DOX-ICI-STH was significantly smaller than DOX-STH, similar to the growth curve analysis results. From these results, it was found that the DOX-ICI-STH group with both DOX and ICI, representing different therapeutic mechanisms, had the highest survival rate, the smallest residual tumor size, and supported not only tumor cell death but also inflammatory cell infiltration into and around the

Furthermore, immunofluorescence staining was performed to analyze how tumor cell death (TUNEL), tumor cell proliferation (Ki67), and cytotoxic T-cell infiltration (CD8) changed upon DOX-ICI-STH treatment of Hepa 1–6 tumor model (Figure 8). Relative to TUNEL staining to analyze apoptotic cell death (Figure 8A), the control and STH groups showed no significant difference. However, all drug-treated groups showed a significant increase in TUNEL-positive cells compared to the control group. The DOX-STH group showed a high and significant increase in TUNEL-positive cells compared to the STH and ICI-STH groups. Interestingly, the DOX-ICI-STH group, which delivers both DOX and ICI, showed a significant increase in TUNEL-positive cells compared to all groups (p < 0.01) (Figure 8C).

The expression of the proliferation marker Ki67 was highest in the control group, as opposed to TUNEL (Figure 8B,C). The control and STH groups showed increased Ki67 marker expression compared to the drug-loaded STH groups (DOX-STH, ICI-STH, and DOX-ICI-STH). The DOX-ICI-STH group showed lower Ki67 marker expression compared to DOX-STH. At the same time, the difference between DOX-STH and ICI-STH was not significant.

CD8-positive cytotoxic T-cells, which are known as tumor-killing immune cells, were not well observed in the control and STH groups but showed a significant increase in the treatment groups (DOX-STH, ICI-STH, DOX-ICI-STH) (Figure 8B,C). In particular, the DOX-ICI-STH group showed a significant increase among all treatment groups. These results suggest that the combined delivery of DOX and aPD-1 causes an increase in apoptotic

tumor cell death, a decrease in proliferative cells, and an increase in the infiltration of cytotoxic T-cells.

3. Conclusion

Our transformative technology, a catheter-based locoregional approach utilizing the DESTH, holds great promise as a nextgeneration TACE option for HCC treatment. It is worth noting that the STH was recently approved by the FDA (July, 2022: Class II Vascular Embolization Device) as an embolic agent. Additionally, by addressing the limitations of conventional TACE methods, DESTH offers a novel solution to induce more efficient ischemic cell death within the tumor microvasculature while achieving effective co-delivery of chemo- and immunotherapy agents. The sustained and pH-dependent release of DOX and aPD-1 further enhances its potential as a valuable and transformative tool in advancing HCC therapies. The remarkable results obtained in the mouse liver tumor model, including the highest survival rate, smallest residual tumor size, increased tumor cell death, and enhanced inflammatory cell infiltration, underscore the clinical significance of our approach. Immunofluorescence assays revealing an augmented apoptotic tumor cell death, reduced proliferative cells, and heightened cytotoxic T-cell infiltration further emphasize the potential of DESTH in improving HCC treatment outcomes. Overall, the compelling evidence presented here supports the notion that DESTH represents a promising option for enhancing the efficacy and precision of HCC treatment, potentially improving the prognosis and quality of life for HCC patients.

4. Experimental Section

Materials and Cell Lines: Type A porcine skin gelatin, formaldehyde solution (4% v/v), human IL-2 ELISA kit, recombinant human interferongamma (E. coli), Triton X-100, phytohemagglutinin (PHA-P-lectin from Phaseolus vulgaris (red kidney bean)), bovine serum albumin (BSA), Eagle's Minimum Essential Medium (EMEM) with Earle's salts, DOX hydrochloride, and 4',6-diamidino-2-phenylindole (DAPI) for nucleic acid staining were purchased from Sigma Aldrich. Live&Dead cell viability kit, Alexa Fluor 488 phalloidin, Alexa Fluor 568 phalloidin, PrestoBlue cell viability reagent, Honeywell Fluka citric acid/sodium hydroxide buffer solution pH 5.0, Honeywell Fluka potassium dihydrogen phosphate/disodium hydrogen buffer solution pH 7.0, and Dulbecco's phosphate-buffered saline (DPBS; GIBCO) were purchased from Thermo Fisher Scientific. Rat IgG ELISA Kit (ab189578), anti-PD-L1 antibody[38-40] (FITC) (ab224027), anti-Interferon gamma antibody [4S.B3] (ab178447), APC anti-PD1 antibody [EH12.2H7], and recombinant human IgG1 protein (ab155632) were purchased from Abcam. Synthetic nanoclay (Laponite) was purchased from (BYK Additives Ltd, TX, USA). 1 mL BD Luer-Lok and 3 mL BD Luer-Lok syringes were purchased from BD Medical. Cook Beacon Tip 5.0 Fr angiographic catheter was purchased from Cook Medical. Terumo MC*PV2815Y Progreat microcatheter system 2.8 Fr × 3.0 Fr × 130 cm was purchased from DOTMED. Hoechst 33342/PI double staining kit was purchased from Biorbyt. Anti-PD-1 rat monoclonal antibody [clone: RMP1-14] was purchased from Bio X Cell. Glass bottom cell culture dish Φ 15 mm was purchased from NEST Scientific. Corning 24 mm Transwell 0.4 μm polyester membrane was purchased from Costar. Hep G2(HB-8065) was purchased from ATCC, PD-1 stable cell line was a stably transfected CHO-K1 cell line that expressed human PD-1 and was purchased from Abeomics (14-500ACL).

Preparation of Gelatin/Laponite STH: To prepare the gelatin/Laponite STHs, 18% w/v gelatin and 9% w/v Laponite stock solutions were

1616208, 2024, 8, Downloaded from https://davanced.onlinelibrany.wiley.com/doi/10.1002/admf.202309069 by Korea University Library. Wiley Online Library on [2309/2025]. See the Terms and Conditions (https://onlinelibrary.wiley.com/terms-and-conditions) on Wiley Online Library for rules of use; OA articles are governed by the applicable Creative Commons License

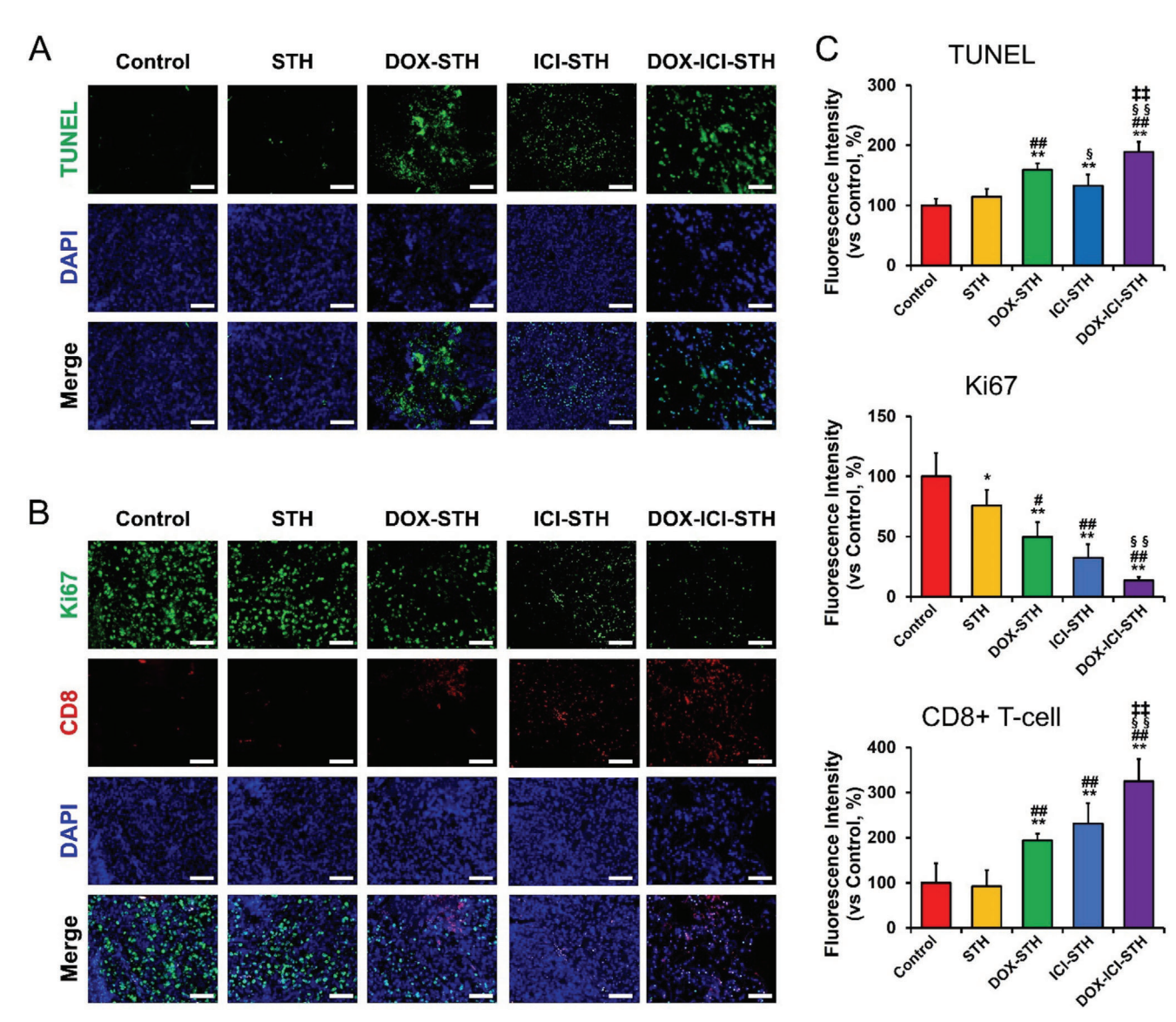


Figure 8. Immunofluorescence staining studies of DESTH on Hepa 1-6 tumor model. A) Representative immunofluorescence images of tumor tissues from Hepa 1-6 mouse tumor model stained with TUNEL (green) and DAPI (blue) to assess apoptotic cell death. Scale bar is 100 μ m. B) Representative immunofluorescence images of tumor tissues stained for Ki67 (green, proliferative cells), CD8 (red, CD8+T cells), and DAPI (blue, nuclei) to assess cell proliferation and immune cell infiltration. C) Quantitative analysis of TUNEL, Ki67, and CD8 immunofluorescence staining. *p < 0.05, **p < 0.01, ANOVA (*: compared to control, #: compared to STH, \P : compared to DOX-STH, and \ddagger : compared to ICI-STH).

prepared separately using ultrapure water. STHs with 6% w/v total solid content and various gelatin/Laponite ratios (1:3, 1:1, 3:1—6NC25, 6NC50, 6NC75) were prepared from the stock solutions following **Table 1**. The stock solutions were mixed with a defined weight of ultrapure water at 3000 rpm for 5 min in a SpeedMixer (DAC 150.1 FVZ, Germany). The mixing step was repeated three times with a 5-min interval between mixings. The gelatin/Laponite STHs were stored at 4 °C for 24 h before use. Before any experimental procedures, the gelatin/Laponite STHs were equilibrated at room temperature (25 °C) for 60 min.

Rheological Characterization: Rheological properties of the STHs, including shear stress, viscosity, and storage moduli, were evaluated using a parallel plate geometry on an Anton Paar rheometer (AR-G2, TA instruments protocol). Mineral oil was added around the plate once the samples were loaded to prevent the hydrogel samples from evaporating throughout the run. Under the application of fixed oscillatory stress of 10 Pa at 25 °C and 01–100 Hz, an oscillatory frequency sweep was achieved. Shear

stress, temperature sweep, viscosity, and storage moduli were measured with a 25 mm sandblasted parallel-plate geometry. Frequency sweeps were

Table 1. Summary of mixed solution ratios for preparing gelatin/Laponite STHs.

Gelatin/Laponite STH formulations			
	6NC25	6NC50	6NC75
Gelatin 18% [g]	12.50	8.33	4.17
Laponite 9% [g]	8.33	16.67	25.00
Water [g]	29.17	25.00	20.83
Total [g]	50.00	50.00	50.00

ADVANCED FUNCTIONAL MATERIALS 1616282, 2024, 8, Downloaded from https://divanced onlinelibrary.wiely.com/doi/10.002/admf.n202399069 by Korea University Library, Wiley Online Library on [2309/2025]. See the Terms and Conditions (https://onlinelibrary.wiely.com/erms-and-conditions) on Wiley Online Library for rules of uses; OA articles are governed by the applicable Creater Commons

performed at 0.1–10 Hz under a fixed oscillatory strain of 1% at 25 °C. Temperature sweeps were performed at 1 Hz and a fixed strain of 1% from 10–40 °C. Viscosity experiments were performed at 25 °C with a 0.001–10 1/s shear rate. Oscillatory step strain experiments were performed at 1 Hz at 25 °C with cycles 1, 3, and 5 at a strain of 1% and cycles 2 and 4 at 200% strain

Injectability Assessment of Gelatin/Laponite STH: For injectability assessment, gelatin/Laponite STHs were loaded into 1 cc or 3 cc syringes and injected through 2.8 Fr or 5.0 Fr microcatheters (1 cc-2.8 Fr, 3 cc-5.0 Fr). The injection forces were examined by a mechanical tester (Instron 5943, Instron Int. Ltd., MA, USA) using the Bluehill version 3 software with a 100 N load cell and an injection rate of 100 mm min⁻¹.

Loading of DOX and aPD-1 within STH: STHs were thoroughly mixed with different amounts of aqueous DOX solution (Oakwood Chemical, SC, USA) of 10 mg mL $^{-1}$ in a SpeedMixer at 3000 rpm for 5 min to achieve an even distribution of the components, resulting in final concentrations of 1, 10, 100, and 1000 mg g $^{-1}$. aPD-1 was added to achieve a concentration of 100 µg g $^{-1}$.

Chemotherapy and Immunotherapy Release Studies: The DESTHs were analyzed by releasing DOX and a-PD1 against physiologically neutral and acidic buffers. The DESTHs were submerged in buffers with predetermined pH levels of 5.0 and 7.4. The DOX concentrations following release were determined by measuring the fluorescence at an excitation of 470 nm and an emission of 560 nm at specific time intervals. The solution was taken at time points of up to 28 days to quantify DOX release into the surrounding buffer, and DOX fluorescence was measured using the fluorometer. For the aPD-1 release assessment, a rat IgG ELISA kit was used. A standard curve was generated for both.

DOX-STH Anticancer Assessment In Vitro: HepG2 cells were cultured in DMEM supplemented with 10% FBS and 1% streptomycin/penicillin solution at 37 °C under a 5% CO2 atmosphere. Subculturing was performed using trypsin EDTA (Gibco, CA, USA) once the cells achieved 80–90% confluency and then seeded at 5 \times 10⁴ cells per well on a 24-well plate (Corning, USA). After 1 day of culture, the eluates (8 g of drug-loaded STH with 40 mL of media on top) of the DOX release from the STHs were added to the cells. Cell viability was assessed using a Live/Dead viability/cytotoxicity kit (Invitrogen, USA) after incubating the cells for 1, 3, or 7 days. A fluorescence microscope (Zeiss Axio Observer; Carl Zeiss, Plan, Germany) was used to conduct imaging. Using the Image J software (NIH, MD, USA), ten non-overlapping areas at 20 \times magnification were utilized for quantitative data analysis. The living-to-total cell number ratio was taken to calculate the viability of cells (%).

In Vitro Release Study of aPD1 from DESTHs with CHO PD1 Cell Line: Eluates from media (days 1, 3, 7, 10, and 14) from varying DESTH formulations (6NC25, 6NC50, 6NC75) loaded with 100 $\mu g \, g^{-1}$ of DOX were prepared for each predetermined sample composition. The eluates were then exposed to the PD-1 stable cell line, and an FC blocker was added to each tube (150 uL per tube). After 1 h of incubation, 200 mL of diluted antimouse IgG antibody (Alexa Fluor 488) (abcam ab150113) (ratio of 1:1000) was added to each epitube. The samples were again incubated before 1 mL of DPBS was added. The samples were read on a Flow cytometer (Attune Thermo Fisher) to investigate the binding events, and the results were analyzed using the FloJo Software.

In Vivo Assessment of Antitumor Efficacy: 6-week-old male C57B1/6J mice were received from Jackson Laboratories (Bar Harbor, ME, USA). All animal procedures were conducted under the supervision of the IACUC committee of the Lundquist Institute (#22813). In both the survival and tumor growth studies, tumor cells were implanted under general inhalation anesthesia. Anesthesia was induced using isoflurane (isoflurane concentration: 5% for induction/2–3% for maintenance, oxygen flow: 2 L min⁻¹), and the depth of anesthesia was maintained by continuous anesthetic gas supply through a face mask and spontaneous inspiration. The hair at the injection site was shaved with a clipper, disinfected with alcohol and povidone, and 1×10^6 Hepa 1–6 cells were injected subcutaneously into the flank. When the tumor volume reached $\approx 50-200$ mm, [3] 50 uL of experimental material was injected into the tumor. The negative control group (Tumor) was injected with DPBS. Blank STHs (6NC25), DOX-STH (DOX conc: 5 mg kg⁻¹), ICI-STH (aPD-1: 5 µg kg⁻¹), and DOX + ICI-loaded

STHs (5 mg kg^{-1} of DOX and 5 $\mu g \ kg^{-1}$ of aPD-1) were injected into the tumor.

For the survival study, five mice from each group were tested to assess the survival rate throughout the experimental period. The endpoint of the experiment was defined as a humane endpoint or when the maximum length of the tumor was greater than 15 mm. Animals that met the endpoint criteria were humanely euthanized and considered "dead." For the tumor growth study, tumor size was measured using a caliper every 2 days, with the final size measurement date set at 16 days after treatment. The humane endpoint was defined as when the tumor size reached over 2000 mm³, or when the criteria for humane endpoint were met. However, no individual animal had a tumor size greater than 2000 mm³ and no individual was satisfied with a human endpoint such as tumor ulceration, anorexia, or cachexia. Five mice from each experimental group were euthanized by CO₂ inhalation on postoperation day 16 for the tumor growth curve analysis. Tissue samples including tumor (with adjacent skin), liver, lung, heart, spleen, and kidney were taken from each group and fixed in 10% neutralized buffered formalin (NBF, Leica Biosystems, IL, USA) for further histopathological evaluation.

Histopathological Evaluation: Tissue samples fixed in NBF were subjected to routine paraffin-based histopathologic procedures (tissue trimming, dehydration, clearing, paraffin infiltration, and paraffin block preparation). Tissue paraffin blocks were then subjected to standard hematoxylin (Leica Biosystems) and eosin (Sigma) (H&E) staining after tissue sections were cut to 4 um thickness using a microtome. The stained tissue slides were embedded, and microscopic images were obtained using a slide scanner (PathScan Enabler 5, Meyer, USA) and a Zeiss inverted microscope. Quantification analysis of the tumor area was obtained using AmScope image analysis software (Irvine, CA, USA) on whole mount images. Image J image analysis software (NIH, MD, USA) was used to quantify the number of positive cells/intensity in immunofluorescence images.

Deparaffinized tissue slides were subjected to a heat-induced antigen retrieval process to liberate antigens for immunostaining. The slides were then permeabilized in 0.3% Triton in DPBS and blocked with 1% bovine serum albumin for 30 min. The primary antibodies used were: An anti-Ki67 rabbit polyclonal antibody (Abcam, CA, USA), anti-CD8 mouse polyclonal antibody (Abcam), and BrdU-FITC TUNEL assay kit. The primary antibodies were incubated overnight at 4 °C. The antibodies used as secondary antibodies were fluorescence labeled: goat anti-mouse IgG Alexa Flour 594 conjugated antibody (ThermoFisher) and goat anti-rabbit IgG Alexa Flour 488 conjugated antibody (ThermoFisher). To prevent fluorescence bleeding and for counterstaining, the slides were embedded with fluoromounts containing DAPI (Vector Laboratories, CA, USA). The stained slides were placed under an inverted fluorescence microscope (Axio Observer 5, Zeiss, Germany) to obtain fluorescence images.

Statistical Analysis: All data were presented using average \pm standard deviation. More than a triplicate of group data sets was used for statistical analysis. Multiple comparisons were conducted using one-way ANOVA with Bonferroni post hoc tests. p < 0.05 was deemed to be statistically significant.

Supporting Information

Supporting Information is available from the Wiley Online Library or from the author.

Acknowledgements

The authors gratefully acknowledge funding from the National Institutes of Health (CA257558, DK130566). N.F. appreciates the postdoctoral fellowship (PDF) from the National Science and Engineering Research Council (NSERC). H.-J.K. would like to acknowledge the Basic Science Research Program through the National Research Foundation of Korea (NRF), funded by the Ministry of Education (RS-2023-00240729). This research was supported by the MSIT (Ministry of Science and ICT), Korea, under the ITRC (Information Technology Research Center) support

16163028, 2024, 8, Downloaded from https://advanced.onlinelibrary.wiley.com/doi/10.1002/adfm.202309069 by Korea University Library, Wiley Online Library on [23/09/2025]. See the Terms and Conditions (https://onlinelibrary.wiley.com/erms

litions) on Wiley Online Library for rules of use; OA articles are governed by the applicable Creative Common

program (IITP-2023-RS-2023-00258971) supervised by the IITP (Institute for Information & Communications Technology Planning & Evaluation). This research was also supported by the Korea University grant (KU S-FRG, K2319831) and the National Research Foundation (NRF) of Korea (2019R1A6A1A03031807).

Conflict of Interest

A.K. was co-founder of a start-up (Obsidio, Inc.) based on an STH for biomedical applications that Boston Scientific recently acquired.

Data Availability Statement

The data that support the findings of this study are available in the supplementary material of this article.

Keywords

drug delivery, hydrogel biomaterials, immunotherapy, Laponite, liver cancer, shear-thinning

> Received: August 2, 2023 Revised: September 18, 2023 Published online: October 10, 2023

- [1] C. Yang, H. Zhang, L. Zhang, A. X. Zhu, R. Bernards, W. Qin, C. Wang, Nat. Rev. Gastroenterol. Hepatol. 2023, 20, 203.
- [2] J. M. Llovet, R. K. Kelley, A. Villanueva, A. G. Singal, E. Pikarsky, S. Roayaie, R. Lencioni, K. Koike, J. Zucman-Rossi, R. S. Finn, Nat. Rev. Dis. Primers 2021, 7, 6.
- [3] M. Le Grazie, M. R. Biagini, M. Tarocchi, S. Polvani, A. Galli, World J. Hepatol. 2017, 9, 907.
- [4] D. Suresh, A. N. Srinivas, A. Prashant, K. B. Harikumar, D. P. Kumar, Clin. Exp. Med. 2023, 1.
- [5] A. Saito, H. Toyoda, M. Kobayashi, Y. Koiwa, H. Fujii, K. Fujita, A. Maeda, Y. Kaneoka, S. Hazama, H. Nagano, A. H. Mirza, H.-P. Graf, E. Cosatto, Y. Murakami, M. Kuroda, Mod. Pathol. 2021, 34, 417.
- [6] J. Guo, S. Wang, Y. Han, Z. Jia, R. Wang, Oncol. Lett. 2021, 22, 554.
- [7] J.-L. Raoul, A. Forner, L. Bolondi, T. T. o. Cheung, R. Kloeckner, T. De Baere, Cancer Treat. Rev. 2019, 72, 28.
- H. Albadawi, I. Altun, J. Hu, Z. Zhang, A. Panda, H.-J. Kim, A. Khademhosseini, R. Oklu, Adv. Sci. 20218, 2003327.
- [9] Q. i. Wang, Y. He, M. Shen, L. Huang, L. i. Ding, J. Hu, Y. Dong, H. Fu, Q. Wang, Y. Sun, L. Zhang, J. Cao, Y. Duan, Adv. Funct. Mater. 2021, 31, 2011170.
- [10] Z. Sun, C. Song, C. Wang, Y. Hu, J. Wu, Mol. Pharmaceutics 2019, 17,
- [11] J. Tu, Z. Jia, X. Ying, D. Zhang, S. Li, F. Tian, G. Jiang, Medicine 2016, 95, e560
- [12] A. Poursaid, M. M. Jensen, E. Huo, H. Ghandehari, J. Controlled Release 2016, 240, 414.
- [13] J. Liu, M. Fu, M. Wang, D. Wan, Y. Wei, X. Wei, J. Hematol. Oncol. **2022**, 15, 1,
- [14] D. B. Johnson, C. A. Nebhan, J. J. Moslehi, J. M. Balko, Nat. Rev. Clin. Oncol. 2022, 19, 254.
- [15] R. C. Sterner, R. M. Sterner, Blood Cancer J. 2021, 11, 69.
- [16] M. W. Rohaan, S. Wilgenhof, J. B. A. G. Haanen, Virchows Arch. 2019,
- [17] L. F. Chai, E. Prince, V. G. Pillarisetty, S. C. Katz, Cancer Gene Ther. 2020, 27, 528.

- [18] B. Sangro, P. Sarobe, S. Hervás-Stubbs, I. Melero, Nat. Rev. Gastroenterol. Hepatol. 2021, 18, 525.
- [19] J. A. Seidel, A. Otsuka, K. Kabashima, Trends Immunother. 2017, 1, 2.
- [20] N. Patsoukis, Q. i. Wang, L. Strauss, V. A. Boussiotis, Sci. Adv. 2020, 6, eabd2712.
- [21] A. D. Waldman, J. M. Fritz, M. J. Lenardo, Nat. Rev. Immunol. 2020, 20, 651.
- [22] S. Vafaei, A. O. Zekiy, R. A. Khanamir, B. A. Zaman, A. Ghayourvahdat, H. Azimizonuzi, M. Zamani, Cancer Cell Int. 2022, 22, 2.
- [23] A. Kichloo, M. Albosta, D. Dahiya, J. C. Guidi, M. Aljadah, J. Singh, H. Shaka, F. Wani, A. Kumar, M. Lekkala, World J. Clin. Oncol. 2021, 12,
- [24] A. Haslam, V. Prasad, JAMA Network Open 2019, 2, e192535.
- [25] Y. Shi, D. Li, C. He, X. Chen, Macromol. Biosci. 2021, 21, 2100049
- [26] L. Xie, G. Wang, W. Sang, J. Li, Z. Zhang, W. Li, J. Yan, Q. i. Zhao, Y. Dai, Biomaterials 2021, 269, 120638.
- [27] S. Zhu, T. Zhang, L. Zheng, H. Liu, W. Song, D. Liu, Z. Li, C. Pan, J. Hematol. Oncol. 2021, 14, 156.
- [28] Y. Sun, Y. Liu, X. Ma, H. Hu, Int. J. Mol. Sci. 2021, 22, 6923.
- [29] H. Zhao, L. Wu, G. Yan, Y. Chen, M. Zhou, Y. Wu, Y. Li, Signal Transduction Targeted Ther. 2021, 6, 263.
- [30] S. Yang, M. K. Shim, W. J. Kim, J. Choi, G.-H. Nam, J. Kim, J. Kim, Y. Moon, H. Y. Kim, J. Park, Y. Park, I.-S. Kim, J. u. H. Ryu, K. Kim, Biomaterials 2021, 272, 120791.
- [31] M. Merino, T. Lozano, N. Casares, H. Lana, I. F. Troconiz, T. L. M. Ten Hagen, G. Kochan, P. Berraondo, S. Zalba, M. J. Garrido, J. Nanobiotechnol. 2021, 19, 102.
- [32] S. Zhu, M. Waguespack, S. A. Barker, S. Li, Clin. Cancer Res. 2007, 13,
- [33] Y. u. Chao, Q. Chen, Z. Liu, Adv. Funct. Mater. 2020, 30, 1902785.
- [34] T. Jiang, T. Wang, T. Li, Y. Ma, S. Shen, B. He, R. Mo, ACS Nano 2018, 12, 9693.
- [35] C. Karavasili, D. A. Andreadis, O. L. Katsamenis, E. Panteris, P. Anastasiadou, Z. Kakazanis, V. Zoumpourlis, C. K. Markopoulou, S. Koutsopoulos, I. S. Vizirianakis, D. G. Fatouros, Mol. Pharmaceutics 2019, 16, 2326.
- [36] R. Cui, Q. Wu, J. Wang, X. Zheng, R. Ou, Y. Xu, S. Qu, D. Li, Front. Bioeng. Biotechnol. 2021, 9, 723490.
- [37] J. Ma, B. Wang, H. Shao, S. Zhang, X. Chen, F. Li, W. Liang, Drug Delivery 2022, 29, 1457.
- [38] Q. Wu, M. Qu, H.-J. Kim, X. Zhou, X. Jiang, Y. Chen, J. Zhu, L. Ren, T. Wolter, H. Kang, C. Xu, Z. Gu, W. Sun, A. Khademhosseini, ACS Appl. Mater. Interfaces 2022, 14, 35309.
- [39] C. Loebel, C. B. Rodell, M. H. Chen, J. A. Burdick, Nat. Protoc. 2017, *12*, 1521.
- [40] N. Falcone, N. M. O. Andoy, R. M. A. Sullan, H.-B. Kraatz, ACS Appl. Bio Mater. 2021, 4, 6652.
- [41] M. H. Chen, L. L. Wang, J. J. Chung, Y.-H. Kim, P. Atluri, J. A. Burdick, ACS Biomater. Sci. Eng. 2017, 3, 3146.
- [42] J. Lee, Y. Wang, C. Xue, Y. i. Chen, M. Qu, J. Thakor, X. Zhou, N. R. Barros, N. Falcone, P. Young, F. W. Van Den Dolder, K. Lee, Y. Zhu, H.-J. Cho, W. Sun, B. o. Zhao, S. Ahadian, V. Jucaud, M. R. Dokmeci, A. Khademhosseini, H.-J. Kim, Nanoscale 2022, 14, 350.
- [43] G. Kiaee, N. Dimitrakakis, S. Sharifzadeh, H.-J. Kim, R. K. Avery, K. M. Moghaddam, R. Haghniaz, E. P. Yalcintas, N. R. Barros, S. Karamikamkar, A. Libanori, A. Khademhosseini, P. Khoshakhlagh, Adv. Healthcare Mater. 2022, 11, 2102054.
- [44] C. Xue, H. Xie, J. Eichenbaum, Y. i. Chen, Y. Wang, F. W. Van Den Dolder, J. Lee, K. Lee, S. Zhang, W. Sun, A. Sheikhi, S. Ahadian, N. Ashammakhi, M. R. Dokmeci, H.-J. Kim, A. Khademhosseini, Biotechnol. J. 2020, 15, 1900456.
- [45] C. Bailly, X. Thuru, B. Quesnel, NAR Cancer 2020, 2, zcaa002.
- [46] A. Sheikhi, S. Afewerki, R. Oklu, A. K. Gaharwar, A. Khademhosseini, Biomater. Sci. 2018, 6, 2073.



ADVANCED FUNCTIONA MATERIALS 16163028, 2024, 8, Downloaded from https://advanced.onlinelibrary.wiley.com/doi/10.1002/adfm.202309069 by Korea University Library, Wiley Online Library on [2309/2025]. See

conditions) on Wiley Online Library for rules of use; OA articles are governed by the applicable Creative Commons

www.advancedsciencenews.com www.afm-journal.de

- [47] S. S. Das, Neelam, K. Hussain, S. Singh, A. Hussain, A. Faruk, M. Tebyetekerwa, Curr. Pharm. Des. 2019, 25, 424.
- [48] H. Tomás, C. S. Alves, J. Rodrigues, Nanomedicine 2018, 14, 2407.
- [49] P.-I. Au, S. Hassan, J. Liu, Y.-K. Leong, Chem. Eng. Res. Des. **2015**, 101, 65.
- [50] Z. Cimen, S. Babadag, S. Odabas, S. Altuntas, G. Demirel, G. B. Demirel, ACS Appl. Polym. Mater. 2021, 3, 3504.
- [51] Y. Li, D. Maciel, H. Tomás, J. Rodrigues, H. Ma, X. Shi, Soft Matter 2011, 7, 6231.
- [52] C. M. Tilsed, S. A. Fisher, A. K. Nowak, R. A. Lake, W. J. Lesterhuis, Front. Oncol. 2022, 12, 960317.

- [53] K. Bukowski, M. Kciuk, R. Kontek, Int. J. Mol. Sci. 2020, 21, 3233.
- [54] B. Guiu, E. Assenat, Ann. Transl. Med. 2020, 8, 1693.
- [55] Di Sotto, Irannejad, Eufemi, Mancinelli, Abete, Mammola, Altieri, Mazzanti, D. Giacomo, Int. J. Mol. Sci. 2020, 21, 633.
- [56] M. Mojic, K. Takeda, Y. Hayakawa, Int. J. Mol. Sci. 2017, 19, 89.
- [57] Q. Li, J. Han, Y. Yang, Y. Chen, Front. Immunol. 2022, 13, 1070961.
- [58] D. J. Zabransky, L. Danilova, J. M. Leatherman, T. Y. Lopez-Vidal, J. Sanchez, S. Charmsaz, N. E. Gross, S. Shin, X. Yuan, A. Hernandez, H. Yang, S. Xavier, D. Shu, A. Saeed, K. Munjal, Z. Kamdar, L. T. Kagohara, E. M. Jaffee, M. Yarchoan, W. J. Ho, *Hepatology* 2023, 77, 1566.